# Block Copolymer Self Assembly during Rapid Solvent Evaporation: Insights into Cylinder Growth and Stability

Sean P. Paradiso,[†] Kris T. Delaney,[‡] Carlos J. García-Cervera,[§] Hector D. Ceniceros,[§] and Glenn H. Fredrickson*,[†,‡]

[†]Department of Chemical Engineering, [‡]Materials Research Laboratory, Materials Department, and [§]Department of Mathematics, University of California, Santa Barbara, California 93016, United States

S *Supporting Information*

ABSTRACT: Solvent evaporation has proven to be a remarkably successful tool for directing self-assembly in block copolymers, yet the microscopic mechanisms, processing history dependence and macroscopic control parameters influencing pattern selection remain poorly understood. Here, we leverage dynamical field theory simulations to clarify how copolymer self-assembly proceeds during evaporation. We find that cylinders in the vertical orientation tend to form under modest evaporation rates and relatively weak segregation strengths, and link this behavior to nontrivial, morphology-dependent density correlations present at the ordering front.
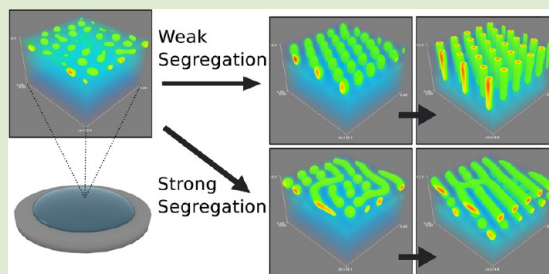
Block copolymers have emerged over the past decade as a versatile platform for a wide range of thin-film technologies including nanofiltration,[1] optical coatings,[2] and lithography.[3] For applications that require patterning nanoscopic pores, such as separation membranes or lithographic masks, cylinder morphologies oriented vertically ($C_\perp$) are required, but often not thermodynamically preferred. In order to meet these design constraints, researchers have turned to solvent-mediated annealing techniques, which offer a number of advantages over conventional thermal annealing, including enhanced defect annihilation kinetics and additional interaction handles for tuning film morphology.[4−10] Still, with the notable exception of works by Osuji and others deploying pressure-driven solvent flows,[11,12] these techniques can, at best, only mitigate the thermodynamic driving force for forming lying-down cylinders ($C_\parallel$), not actively promote a vertical orientation. In their seminal work, Kim and Libera[13] demonstrated that more direct influence over morphology orientation can be achieved by controlling the rate at which solvent-cast films are dried. In their experiments, the equilibrium $C_\parallel$ morphology was observed for modest deswelling rates (∼0.001 mm/min), while increasing to ∼0.003 mm/min led to an unexpected reorientation to $C_\perp$ persisting over a large area. In the wake of this and subsequent work,[7,9] an expectation has developed that rapid evaporation actively drives the growth of vertical cylinders,[14] which an earlier theoretical treatment appears to support.[15] More recent evidence, however, indicates that the degree of perpendicular ordering weakens with increasing evaporation rate beyond a certain threshold.[16] After over a decade of experience, there is still no consistent picture of evaporation-induced ordering in block copolymer systems. While many factors conspire to obscure the fundamental forces involved in this process, slow development is attributed in large part to the black box nature of self-assembly during the solvent removal step.[17] Here, we use a dynamical extension of self-consistent field theory simulations (SI for details) to describe this process and provide a rational basis for designing solvent annealing systems.

Our model describes the self-assembly dynamics of monodisperse diblock copolymers, comprised of chemically distinct A and B type segments in a good, neutral solvent, S. Polymers in the theory are described by continuous Gaussian chains with total length N, unperturbed coil radius $R_g \sim \sqrt{N}$, and minority A-block fraction f_A. All species in the model interact through local, Flory-type contact potentials with strength $\chi_{AB}N$, $\chi_{AS}N$, and $\chi_{BS}N$ for polymer−polymer and polymer−solvent interactions, respectively.[18−20]

When a droplet of dilute copolymer solution is placed in a controlled annealing chamber and exposed to solvent vapor, solvent will enter or leave the film at a rate determined by the difference in solvent chemical potential between the two phases. As solvent leaves the system with time, the total film thickness, here denoted $L(t)$, will decrease to accommodate the lost volume. A simple kinetic model, known as the Hertz-Knudsen relation,[21] provides the evaporative flux (in units of D_0/R_g^4, with D_0 the monomer diffusivity) from any point $\mathbf{r}_{xy}$ on the surface as

$$J_S(\mathbf{r}_{xy}, t) = B_i(\phi_S(\mathbf{r}_{xy}, t) - \phi_S^{eq}) \tag{1}$$

where $\phi_S(\mathbf{r}_{xy})$ is the local solvent fraction, ϕ_S^{eq} is the solvent fraction of a swollen film at equilibrium with the vapor phase, and B_i is a dimensionless mass transfer coefficient relating the
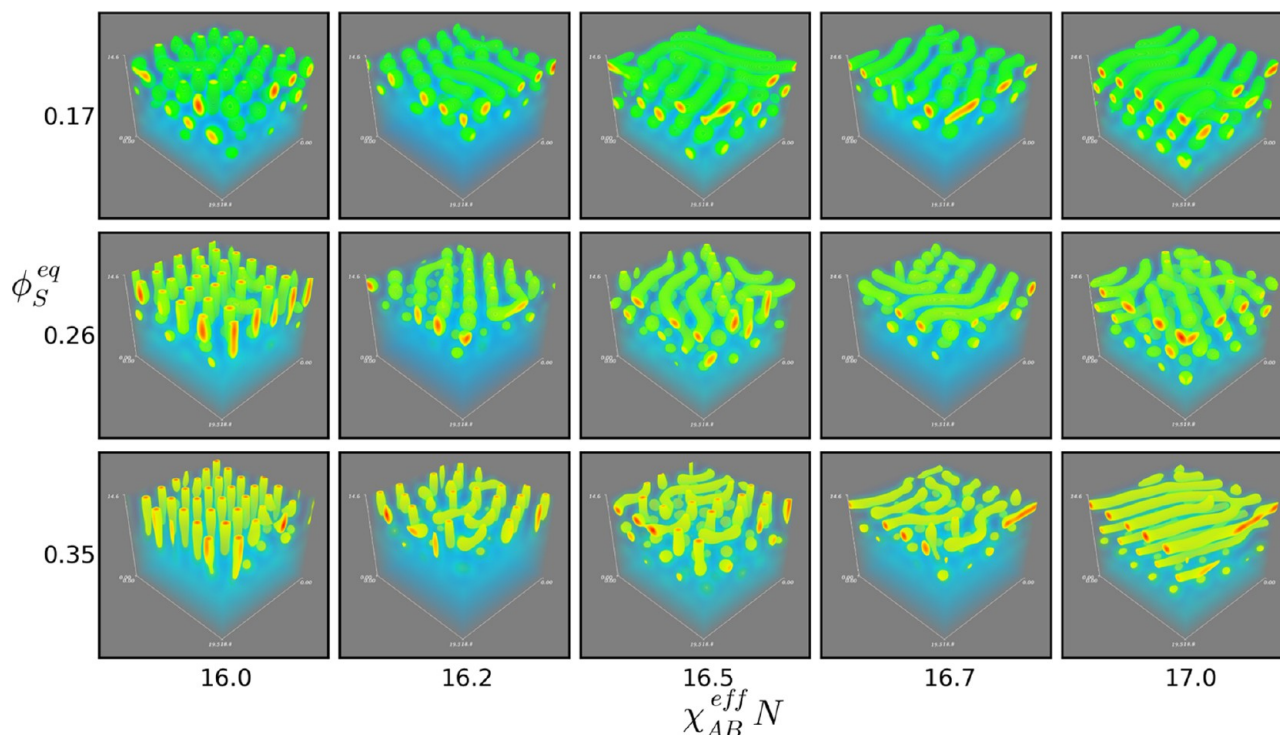
Figure 1. Trends in surface morphology from drying simulations. Shown are snapshots of established surface morphologies extracted from drying simulations while varying the evaporation rate through ϕ_S^{eq} and effective segregation strength through $\chi_{AB}N$. The model parameter $\chi_{AB}N$ was chosen in each simulation by inverting eq 2: $\chi_{AB}N = ((\chi_{AB}^{eff}N)/(1.0 - \phi_S^{eq}))$. Evaporation rate decreases down each column, where we see relatively minor variations in overall morphology at a given $\chi_{AB}N$. In contrast, significant changes are observed with modest increases in $\chi_{AB}^{eff}N$. As the segregation strength is increased, the morphologies transition to primarily $C_{\parallel}$ surface structures through mixed intermediates. Note that only the top portion of the simulation cell is shown. The solvated polymer below the front, while containing essential solvent gradient information for the simulation, has been omitted for clarity.

rate of evaporative loss from the free surface to solvent interdiffusion through the film. The latter parameters, B_i and ϕ_S^{eq}, are the variables used to control evaporation in our simulations. While this model allows for the simulation of preferential wetting conditions observed in experimental systems,[10,22] here we consider the simplest case of a neutral free surface. A more comprehensive study of the parameter space, including surface interactions, will be reported in a following publication. Here, we focus on a model cylinder-forming system with $f_A = 0.3$, $N = 30$, and $B_i = 5$ in order to demonstrate the interplay between evaporation rate (ϕ_S^{eq}) and segregation strength ($\chi_{AB}N$) in determining how ordering proceeds during evaporation.

We begin our discussion of the evaporation process with a visual summary of morphologies obtained from drying simulations over a range of evaporation rates and segregation strengths. We analyze the evaporation process in two parts: first, the onset of ordering at the free surface, followed by the subsequent propagation of order into the film. Importantly, the morphology formed in the initial ordering step is found to be largely determined by the solvent-mediated segregation strength at the surface of the films when ordering begins (Figure 1). Note that in the large B_i limit, fluid near the free surface rapidly equilibrates to the target solvent fraction determined by the parameter ϕ_S^{eq}. In the dilution approximation,[23] the surface solvent concentration (ϕ_S^{eq}) leads to the following effective segregation strength between polymer segments:

$$\chi_{AB}^{eff}N = \phi_P^{eq}\chi_{AB}N = (1 - \phi_S^{eq})\chi_{AB}N \qquad (2)$$

The results in Figure 1 are organized so that the model parameters $\chi_{AB}N$ and ϕ_S^{eq} are not varied independently. Instead, the value of $\chi_{AB}N$ is set such that the derived parameter, $\chi_{AB}^{eff}N$, is held constant down each column. With this parametric constraint, trends suddenly appear where none were forthcoming previously. We find that just as $\chi_{AB}N$ dictates whether a copolymer is ordered or disordered in the melt, its solvated analogue ($\chi_{AB}^{eff}N$) is predictive of the surface morphology that develops as the films are dried. As this factor is increased, morphologies are seen to transition smoothly from primarily $C_{\perp}$ at the surface of the film to $C_{\parallel}$. Importantly, sizable changes in the evaporation rate have evidently minor effect on the pattern selection during this early ordering stage. At first, this may appear to be in disagreement with experimental evidence for ordering transitions driven by changes in the evaporation rate. However, in experimental studies, the evaporation rate is typically varied while other parameters (e.g., $\chi_{AB}N$) are held constant. Recall from above that as ϕ_S^{eq} is lowered, the effective segregation strength increases according to eq 2. While the effects of varying the solvent vapor pressure (ϕ_S^{eq}) and $\chi_{AB}^{eff}N$ are convoluted experimentally, our simulations identify the changes in segregation strength (evaluated at the surface of the film) as the primary factor that determines pattern selection at early stages in the drying process. In order to understand this transition and how the evaporation rate impacts the propagation of order into the film, we take a closer look at the full dynamical trajectories of thin films as they are dried.

Consider the ordering trajectories illustrated in Figure 2. In each case, no ordering is observed until the unstable region near the surface has penetrated a short distance ($\sim 5R_g$) into the
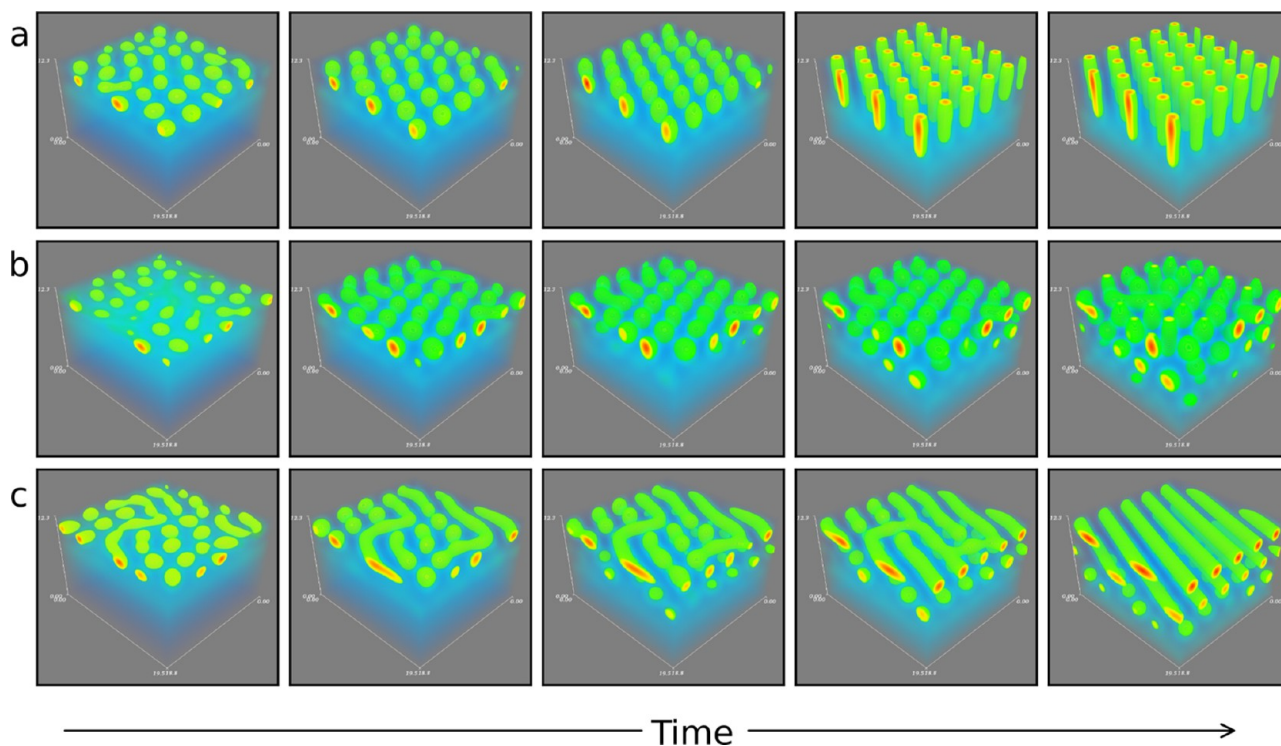
Figure 2. Ordering pathways in drying films. Two primary failure mechanisms deviating from the $C_\perp$ front are shown as they develop. (a) The typical process observed when $C_\perp$ form in drying simulations with $\chi_{AB}^{eff}N = 16.0$, $\phi_S^{eq} = 0.23$. (b) Increasing the evaporation rate from (a) by taking $\phi_S^{eq} = 0.23 \rightarrow 0.17$ leads to the formation of a second layer of spheres beneath the surface morphology, disrupting potential cylinder growth. (c) Increasing $\chi_{AB}^{eff}N \rightarrow 17$ leads to rapid coalescing of spheres at the surface, resulting in a $C_\parallel$ morphology. Simulation parameters $(\phi_S^{eq}, \chi_{AB}^{eff}N)$ used (a) (0.23, 16.0), (b) (0.17, 16.0), and (c) (0.23, 17.0).
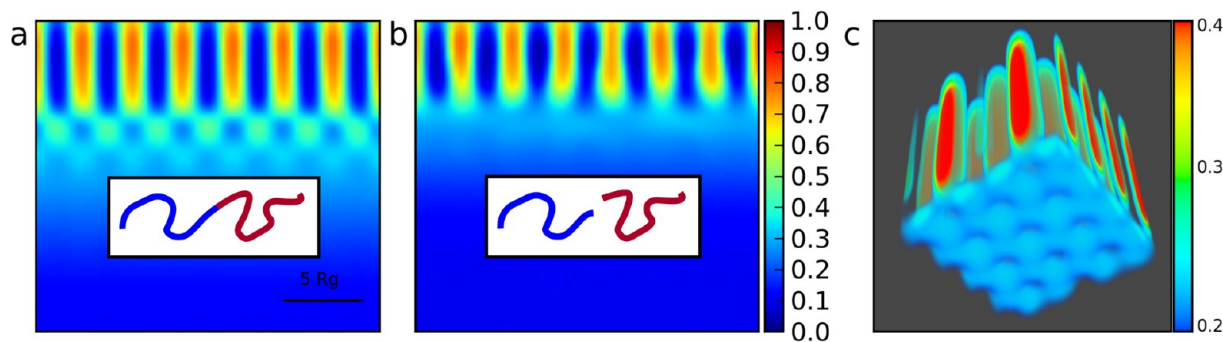

Figure 3. Bonding constraints emerge destabilizing patterns beneath the front. (a) Drying simulations of a symmetric block copolymer ($f_A = 0.5$) system exhibit a regularly patterned response layer at the interface between ordered and disordered fluid. (b) When these simulations are repeated with a symmetric homopolymer blend, no response layer is observed. (c) Ordered $C_\perp$ front (upper, red) and response layer (lower, light blue) from an evaporation simulation of $f_A = 0.3$ diblock copolymers in 3D, seeded with an initially perfect $C_\perp$ structure for illustration. Note that the density scale has been modified in order to visualize the response layer.

film, allowing a single layer of phase-separated spheres to form. This is consistent with expectations derived from the mean-field phase diagram, where the path from the disordered to hexagonal phase is interrupted by a small region of FCC- and BCC-ordered spheres.[20,24] As evaporation proceeds, the defective spheres begin to reorganize onto a hexagonal lattice. At this stage, a bifurcation appears between trajectories that lead to $C_\perp$ and $C_\parallel$ fronts. Since there is a slight time delay before ordering begins, the value of $\chi_{AB}^{eff}N$ at the surface represents how deeply the fluid is quenched into the cylinder region of the phase diagram. Systems at large $\chi_{AB}^{eff}N$ are unable to support the spherical intermediate long enough for this reorganization step to complete, and spheres begin to coalesce to form cylinders in the plane (Figure 2c). Weaker quenches,

such as systems either dried more slowly or that have a lower melt $\chi_{AB}N$, provide the system sufficient time for solvent gradients to advance and spheres to stretch along the vertical axis, the first step in the transition to $C_\perp$. This accounts for the difference in behavior between Figure 2a and c and offers a simple, quasi-equilibrium explanation for why we observe a transition with increasing segregation strength.

A common frustration with solvent evaporation techniques is that while the surface morphology may show signs of hexagonal ordering (e.g., by atomic-force microscopy) the $C_\perp$ morphology often fails to penetrate the entire thickness of the film.[7,10,16] We observe evidence of this behavior as the $C_\perp$-forming system above (Figure 2a) is pushed to a higher evaporation rate (Figure 2b). Under these more rapid drying conditions, the
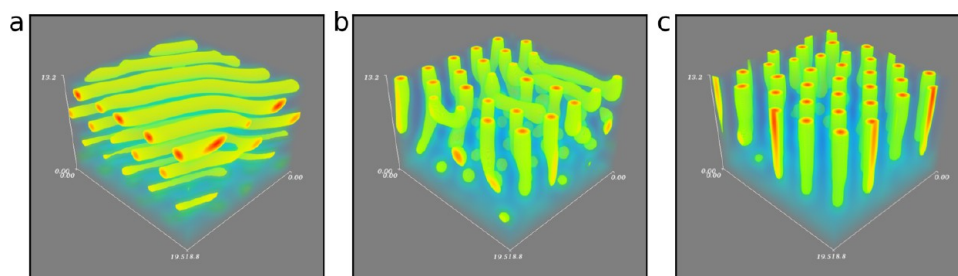
Figure 4. Selective solvent stabilizes $C_\perp$ by weakening the correlation-hole. Solvent quality for the majority block increases from left to right. Because the prepattern present at the leading edge of a $C_\perp$ front is rich in the minority block, a solvent that preferentially swells the majority block inhibits the growth of this mode and enhances the stability of the front. Selectivity is measured by $\Delta\chi_S N = \chi_{AS}N - \chi_{BS}N$, increasing from left to right: (a) −7, (b) 0, (c) 7.

surface morphology fails to establish a coherent front. Instead of growing to form $C_\perp$, the initial surface morphology pinches off from the front as a new layer of spheres begins to form. This is a critical observation, as it is often assumed that once order is established at the free surface, the advancing front will act as a chemical prepattern with which drying fluid may fall into registry. Instead, simulations undergoing rapid evaporation consistently feature a secondary growth mode that competes with the initial patterning at the surface.

This behavior can only be explained by considering the microscopic details underpinning our field theory. To this end, it is helpful to compare the ordering fronts formed beneath solvated homopolymer blend (Figure 3a) and symmetric diblock copolymer (Figure 3b) films. In the case of connected diblock copolymer chains, the perfect ($L_\perp$) pattern in the surface region does not lead to a coherently ordered response layer in the wet film. Rather, a sequence of half-period shifts is observed to bridge the transition from the ordered plug to the disordered polymer beneath the front. We believe these shifts are physical in nature and originate from the self-exclusion phenomenon known as the correlation-hole effect in the scattering theory of block copolymer melts.[20,25] The correlation-hole emerges from the combination of local segment−segment repulsion and the molecular bonding constraint, leading to density correlations on length scales comparable to the random coil radius, R_g. At a patterned interface, these density correlations seed the secondary structures observed in our simulations. Notice that severing the bonding constraint (Figure 3a) and preparing an equivalent homopolymer blend results in loss of structure at the front, confirming that its presence in the diblock case is a direct consequence of the copolymer chain topology. This correlation-hole effect is particularly disruptive for achieving $C_\perp$ order. While the response region attracted to the leading edge of a $C_\parallel$ front is compatible with lying-down cylinders, the pattern formed beneath an array of vertical cylinders (Figure 3c) will not admit simple propagation of $C_\perp$ into the film. However, understanding the presence and origin of these disruptive patterns may allow us to devise formulation adjustments that mitigate their effect.

We conclude with a promising result on the stabilizing effect a majority block-selective solvent has in our simulations. As shown in Figure 4, sweeping the solvent selectivity from weakly favoring the minority to majority block species has a pronounced effect on the quality of vertical cylinders obtained during evaporation. While a rigorous connection remains elusive, it is tempting to explain this behavior in the context of the correlation-hole phenomenon described above. As evident

in Figure 3c, the destabilizing response layer (light blue in the figure) beneath vertically oriented cylinder fronts is rich in polymer segments of the minority block. We suggest that the majority block-selective solvent may be acting to penalize the formation of this response layer, resulting in the enhanced stability observed in our simulations. We note that within the limited data available, majority block-selective solvents have been seen to correlate with perpendicular cylinder formation in drying experiments.[7]

This work has provided the first opportunity to visualize block copolymer self-assembly under rapid evaporation conditions. Our simulations indicate that the resulting morphology depends strongly on the effective segregation strength, $\chi_{AB}^{eff}N$, near the surface of the film. When films are dried too rapidly, however, even modest surface segregation strengths fail to achieve stable growth of $C_\perp$, owing to a dynamical instability observed at the ordering front. Tracing the origin of this instability to the correlation-hole opens up exciting new opportunities for guiding the self-assembly process, such as including selective solvents or blend additives that have been shown to weaken correlations observed at the front.[26] Given this understanding, it would be of interest to examine whether chain architecture (e.g., triblock vs diblock chains), which is at the heart of these competing correlations, can be exploited to promote desired ordering pathways. While we have focused on the problem of aligning vertical cylinders, this work illustrates fundamental aspects of ordering during solvent evaporation, which may prove essential for understanding evaporation-induced self-assembly in broader classes of nanostructured soft materials.

■ ASSOCIATED CONTENT

Ⓢ Supporting Information

Modeling details, including dynamical equations and numerical strategies. This material is available free of charge via the Internet at http://pubs.acs.org.

■ AUTHOR INFORMATION

Corresponding Author
*E-mail: ghf@mrl.ucsb.edu.

Notes
The authors declare no competing financial interest.

■ ACKNOWLEDGMENTS

■ REFERENCES

(1) Jackson, E.; Hillmyer, M. *ACS Nano* **2010**, *4*, 3548−53.

(2) Joo, W.; Park, M. S.; Kim, J. K. *Langmuir* **2006**, *22*, 7960−3.

(3) Glass, R.; Möller, M.; Spatz, J. P. *Nanotechnology* **2003**, *14*, 1153−1160.

(4) Oss-Ronen, L.; Schmidt, J.; Abetz, V.; Radulescu, A.; Cohen, Y.; Talmon, Y. *Macromolecules* **2012**, *45*, 9631−9642.

(5) Huang, H.; Zhang, F.; Hu, Z.; Du, B.; He, T.; Lee, F. K.; Wang, Y.; Tsui, O. K. C. *Macromolecules* **2003**, *36*, 4084−4092.

(6) Brinker, C. J.; Lu, Y.; Sellinger, A.; Fan, H. *Adv. Mater.* **1999**, *11*, 579−585.

(7) Phillip, W. A.; O'Neill, B.; Rodwogin, M.; Hillmyer, M. A.; Cussler, E. L. *ACS Appl. Mater. Interfaces* **2010**, *2*, 847−853.

(8) Jung, A.; Filiz, V.; Rangou, S.; Buhr, K.; Merten, P.; Hahn, J.; Clodt, J.; Abetz, C.; Abetz, V. *Macromol. Rapid Commun.* **2013**, *34*, 610−5.

(9) Kim, S. H.; Misner, M. J.; Xu, T.; Kimura, M.; Russell, T. P. *Adv. Mater.* **2004**, *16*, 226−231.

(10) Albert, J. N. L.; Epps, T. H., III *Mater. Today* **2010**, *13*, 24−33.

(11) Osuji, C. O. *Macromolecules* **2010**, *43*, 3132−3135.

(12) Tran-Ba, K.-H.; Finley, J. J.; Higgins, D. A.; Ito, T. *J. Phys. Chem. Lett.* **2012**, *3*, 1968−1973.

(13) Kim, G.; Libera, M. *Macromolecules* **1998**, *31*, 2569−2577.

(14) Hamley, I. *Nanotechnology* **2003**, *14*, R39−R54.

(15) Phillip, W. A.; Hillmyer, M. A.; Cussler, E. L. *Macromolecules* **2010**, *43*, 7763−7770.

(16) Albert, J. N. L.; Young, W.-S.; Lewis, R. L.; Bogart, T. D.; Smith, J. R.; Epps, T. H. *ACS Nano* **2012**, *6*, 459−66.

(17) Sinturel, C.; Vayer, M.; Morris, M.; Hillmyer, M. *Macromolecules* **2013**, *46*, 5399−5415.

(18) Bates, F. S.; Fredrickson, G. H. *Annu. Rev. Phys. Chem.* **1990**, *41*, 525−57.

(19) Fredrickson, G. H.; Bates, F. S. *Annu. Rev. Mater. Sci.* **1996**, *26*, 501−550.

(20) Leibler, L. *Macromolecules* **1980**, *13*, 1602−1617.

(21) Prosperetti, A.; Plesset, M. *Phys. Fluids* **1984**, *27*, 1590−1602.

(22) Fasolka, M. J.; Mayes, A. M. *Annu. Rev. Mater. Res.* **2001**, *31*, 323−355.

(23) Helfand, E.; Tagami, Y. *J. Chem. Phys.* **1972**, *56*, 3592−3601.

(24) Matsen, M.; Schick, M. *Phys. Rev. Lett.* **1994**, *72*, 2660−2663.

(25) Gennes, P. D. *Scaling Concepts in Polymer Physics*; Cornell University Press: New York, 1979.

(26) Bates, F. S. *Macromolecules* **1987**, *20*, 2221−2225.